sciendo

Local aromaticity of linear *cata*-benzocoronenes and acenes: density functional study

Denisa Cagardová, Peter Poliak, Vladimír Lukeš

Institute of Physical Chemistry and Chemical Physics, Faculty of Chemical and Food Technology, Slovak University of Technology in Bratislava, Radlinského 9, SK-812 37 Bratislava, Slovakia
denisa.cagardova@stuba.sk

Abstract: A computational study using density functional theory is reported for the coronene monomer and selected linear *cata*-benzocoronene oligomers. Local aromaticity was discussed and analysed using the theoretical Harmonic Oscillator Model of the Electron Delocalisation (HOMED) index and its geometric (GEO) and energetic (EN) contributions. The [n]acenes (n = 3, 7, 11 and 15) served as reference molecules. Local aromaticity of individual superbenzene rings has oscillating character. On the other hand, the highest HOMED parameters which are practically independent on the molecular lengths were found for the smallest molecules including condensed benzene rings in their structure. For the largest structure of [n]acenes (n = 15), the inner rings are less aromatic than the outer ones. Depending on the molecular length, the energy gaps between the B3LYP energy levels of the highest occupied and lowest unoccupied molecular orbitals vary from 2.71 eV to 4.04 eV for coronene series and from 0.61 eV to 3.59 eV for [n]acenes.

Keywords: coronene, *cata*-benzocoronene, acene, aromaticity index, HOMED, PAH

Introduction

Polycyclic aromatic hydrocarbons (PAHs) are organic compounds containing multiple aromatic rings made of carbon and hydrogen atoms only (Fetzer, 2000; Haynes, 2011). The main source of PAHs is coal and tar deposits, but they can also be produced by incomplete combustion of organic matter. All PAHs are non-polar and possess typical aromatic electron delocalisation. The simplest examples of these chemicals are [n]acenes, planar benzenoid hydrocarbons with linearly condensed benzene rings, i.e. naphthalene, anthracene, tetracene, pentacene and hexacene. The [n]acenes exhibit increasing reactivity with the increasing number of rings. It is reported that the higher [n]acenes are unstable under light (Dabestani, 1999) and air oxygen exposure (Clar, 1939). Peri-fused benzene rings represent other interesting PAHs. The simplest representative with six rings is coronene, also known as superbenzene with the superaromatic structure (Aihara, 2003). This compound has yellow colour and dissolves in common non-polar solvents, e.g. benzene, toluene, and dichloromethane. Interestingly, coronene occurs naturally as the very rare mineral carpathite which is characterised by flakes of pure coronene embedded in sedimentary rock (Potticary et al., 2017). Coronene is also produced in the petroleum-refining process of hydrocracking where it can dimerize to form a 15-ring, brick-red solid dicoronylene. Thermal pyrolysis of coronene generates several condensed trimer, tetramer, and pentamer coronenes with black colour. From the technological point of view, the formation of coronene oligomers in hydrocracking reactors is a serious problem because its low solubility makes it precipitate in any cooler part of the reactor flow path (Mackay and Callcott, 1998). On the other hand, the large size and molecular planarity of coronene and dicoronylenes make them promising as chromatographic separation materials (Kiyokatsu et al., 1990). They can also be used as solvent probes, e.g. pyrene. Interestingly, dicoronylene has been studied as a model for interstellar PAHs (Clar, 1939).

The concept of aromaticity is fundamental for the rationalisation and understanding of the structure and reactivity of about two-thirds of all known chemical species. To better understand this phenomenon, compounds with condensed benzene rings have been studied by many theoretical and organic chemists. Electronic structure of aromatic molecules can be investigated and described using several different techniques, such as the study of ring currents (Steiner and Fowler, 1996; Anusooya et al., 1998, Ligabue et al., 1999), calculation of resonance energies (Behrens et al., 1994; Moyano and Paniaguya, 1993) and the analysis of several aromaticity indicators, e.g. Harmonic Oscillator Model of Aromaticity (HOMA) Index (Schleyer et al., 2001; Krygowski and Cyrański, 2001), multiple charge density properties derived from the Atoms-in-Molecules (AIM) theory (Howard and Krygowski, 1997) or graph theory-based descriptors (Randic, 2003). The Density Functional Theory (DFT) represents a quantum chemical

approach for the frontier molecular orbital energy modelling of conjugated systems with acceptable computational cost (Hohenberg et al., 1964; Runge and Gross, 1984). The DFT method is convenient for the gas-phase optimal geometry investigation of large molecules since it includes the effect of electron correlation. Local aromaticity of simple six-membered rings in three series of benzenoid compounds, namely, [n]acenes, [n]phenacenes, and [n]helicenes for n = 1 to 9, has been assessed by Portella et al (Portella et al., 2005). This DFT study showed that local aromaticity in [n]acenes increases steadily from the peripheral to the central rings. For [n]phenacenes, all aromaticity indicators show that external rings are the most aromatic. Although the local aromaticity changes related to the elongation of the molecular chain, the acenic structures were well characterised; systematic comparative studies of hydrocarbons with circular formation of benzene rings are less discussed in literature.

Experimental energies of frontier molecular orbitals (MOs) are frequently obtained from the first electrochemical reduction peak and the lowest energy optical band gap. Therefore, theoretical analysis of the lowest vertical energy optical transitions is necessary for proper determination of the optical band gap.

With respect to this fact, theoretical analysis of the electronic structure of the model series of *cata*-benzocoronene oligomers made of up to four coronene units linearly *cata*-condensed with a benzene unit (Fig. 1) is presented. Partial goals of this study are: (1) to calculate optimal geometries; (2) to evaluate energies of the frontier molecular orbitals and (3) to calculate the lowest energy optical transitions. Finally, DFT parameters for the evaluation of aromaticity indices are suggested. Consequently, local aromaticity of the studied coronene series will be discussed and compared with the reference [n] acenes (n = 3, 7, 11 and 15).

Theoretical and computational methodology

Quantum chemical calculations were performed using the Gaussian 09 program package (Frisch et al., 2010). Optimal geometries of the studied molecules in the electroneutral state were calculated by the DFT method with B3LYP functional (Becke's three parameter Lee–Yang–Parr) (Lee et al., 1988; Becke, 1988) and Hartree-Fock exchange functional M06-2X (Zhao and Truhlar, 2008) without any constraints (energy cut-off of 10^{-5} kJ·mol^{-1}, final RMS energy gradient below 0.01 kJ·mol^{-1}·A^{-1}). The 6-31G(d,p) basis set of atomic orbitals was applied for all atoms (Hariharan and Pople, 1973; Rassolov et al., 1998). The optimised structures were confirmed to be true minima by vibrational analysis (no imaginary frequencies). On basis of the optimised geometries, 25 vertical transition

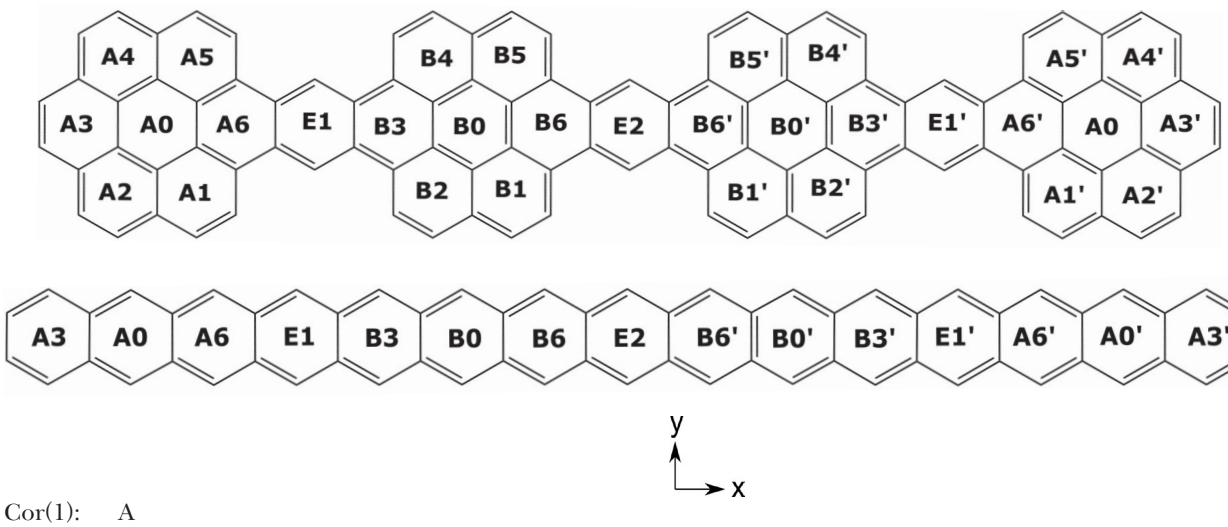

Cor(1):	A														
Cor(2):	A	E1	A'												
Cor(3):	A	E1	B	E1'	A'										
Cor(4):	A	E1	B	E2	B'	E1'	A'								
Ac(3):	A3	A0	A6												
Ac(7):	A3	A0	A6	E1	A6'	A0'	A3'								
Ac(11):	A3	A0	A6	E1	B3	B0	B6	E1'	A6'	A0'	A3'				
Ac(15):	A3	A0	A6	E1	B3	B0	B6	E2	B6'	B0'	B3'	E1'	A6'	A0'	A3'

Fig. 1. Schematic structure and notation of studied coronene, *cata*-benzocoronene oligomers and [n]acenes. Individual aromatic rings are denoted by capital letters.

energies and oscillator strengths between the initial and the final electronic states were computed by the time dependent (TD)-DFT method (Ahlrichs and Furche, 2002). In case of B3LYP geometries, the range-separated functional CAM-B3LYP (Yanai et al., 2004) was also used in the calculations of optical transitions. The molecules and molecular orbitals were visualised using the Molekel program package (Flukiger et al., 2002).

Results and Discussion

Structural aromaticity indices and local aromaticity

Aromaticity is a multidimensional property and aromatic compounds are very often characterised by different sets of indices based on various physical properties (Cyrański et al., 2002). As a structure-based measure, geometrical changes of carbon-carbon bond lengths with respect to the structural changes were expressed using the Harmonic Oscillator Model of Electron Delocalisation (HOMED) index (Frizzo and Martins, 2012)

$$\mathrm{HOMED} = 1 - \frac{\alpha}{n}\left\{\sum_{i=1}^{n}\left(R_{ref} - R_i\right)^2\right\} \qquad (1)$$

where n represents the number of bonds considered and R_i is the actual bond length. The empirically determined parameter α = 257.7 Å^{-2}, and the optimal reference bond length R_{ref} = 1.388 Å. These parameters were suggested from the analysis of X-ray structures of a large set of organic molecules (Krygowski and Cyrański, 2001). Nevertheless, a combination of the DFT R_i bond lengths with these empirical parameters can lead to an undesirable HOMED parameter value for benzene lower than 1. To eliminate this problem, these parameters were evaluated using the DFT calculation in the 6-31G(d,p) basis set. Optimised carbon-carbon bond lengths of the benzene molecule are 1.3963 Å for B3LYP and 1.3928 Å for M06-2X. Normalisation constant α was calculated from Eq. 2 (Ośmiałowski et al., 2006)

$$\alpha = 2\left\{\left(R_{ref} - R_{sin}\right)^2 + \left(R_{ref} - R_{doub}\right)^2\right\}^{-1} \qquad (2)$$

where the reference single bonds, R_{sin}, and the reference double bonds, R_{doub}, were estimated from ethane and ethene molecules, respectively. The calculated single C—C bond lengths are 1.5300 Å for B3LYP and 1.5259 Å for the M06-2X functional. The C=C double bond lengths are shorter, i.e. 1.3302 Å for B3LYP and 1.3267 Å for M06-2X. Based on these bond lengths, values of the normalisation constant α are 90 Å^{-2} and 91 Å^{-2} for the B3LYP and M06-2X functional, respectively.

Optimal geometries of all studied molecules in the electroneutral state are planar and symmetric. Therefore, aromaticity is affected by the bond length changes within these structures. A comparison of theoretical and X-ray bond lengths for the smallest investigated molecules is presented in Fig. 2. All bond lengths for both functionals are evidently within the reference R_{sin} and R_{doub} bond lengths. In case of superbenzene, the molecule possesses the D_{6h} symmetry and the bond lengths of central ring A0 are 1.428 Å for B3LYP and 1.426 Å for M06-2X. The anthracene molecule has lower symmetry (D_{2h}) and the central ring A0 has four equivalent C—C bonds with the length of 1.400 Å and two equiva-

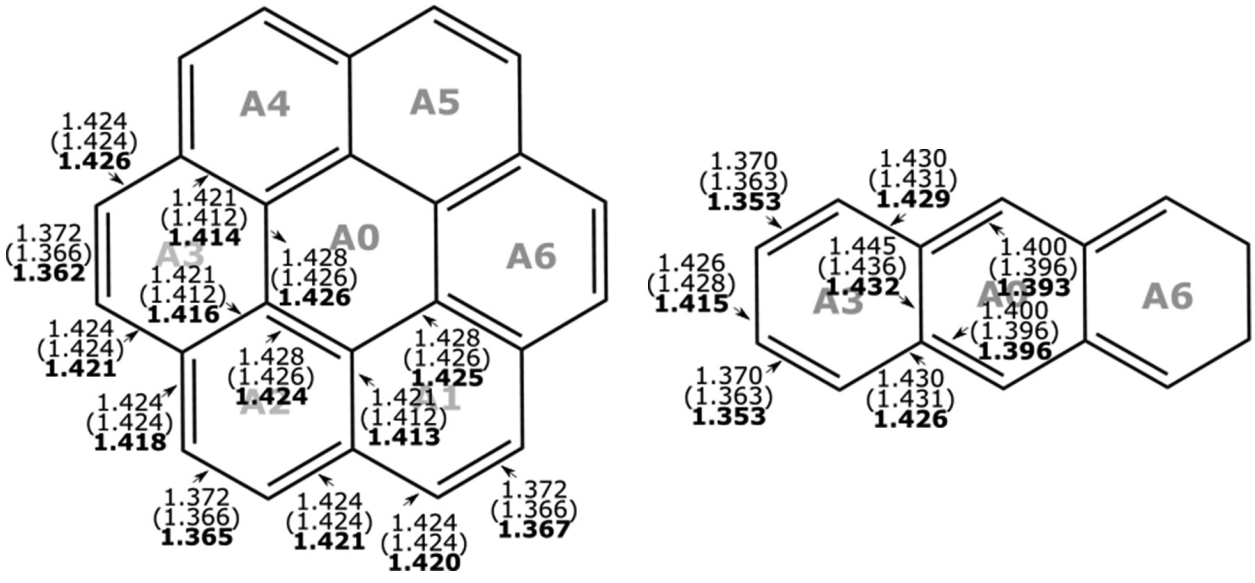

a) b)

Fig. 2. B3LYP, M06-2X (in parentheses) and X-ray (numbers in bold) (Brock and Dunitz, 1990; Potticary et al., 2016) bond lengths of coronene (a) and anthracene (b). Distances are in Angstroms.

lent C—C bonds with the length of 1.445 Å for the B3LYP functional. On the other hand, the M06-2X functional indicates slightly shorter bond lengths: four equivalent bond lengths of 1.396 Å and two equivalent bond lengths of 1.436 Å. A comparison of neighbouring bond lengths revealed that both DFT functionals can offer a difference of up to 0.009 Å which can lead to direct influence on the structural aromaticity indices. Interestingly, X-ray structures of coronene (Potticary et al., 2016) and anthracene (Brock and Dunitz, 1990) have lower symmetry and the C—C bonds distances are closer to the M06-2X results (see Fig. 2).

HOMED parameters evaluated for the central molecular rings of coronene series (lying in the longest axial direction) and acenes exhibit differences in the π-electron delocalisation between the fused outer and inner six-membered rings. As illustrated in Fig. 3, the anthracene molecule exhibits the highest B3LYP HOMED index (0.95) for the central ring A0, while the outer rings are less aromatic (HOMED = 0.90). Local aromaticity increase from the edge to the centre can similarly be observed for heptacene Ac(7). According to Portella et al. (Portella et al., 2005), local aromaticity of the peripheral and central rings decreases for acenes with higher number of rings (n > 7). In case of the coronene series, local aromaticity of individual central aromatic rings (A0/A0', B0/B0', E1/E1' and E2) has an oscillating character. Interestingly, the highest B3LYP HOMED parameters (0.97) were found for the connecting benzene rings E1/E1' and E2. For better understanding of local aromaticity changes, the HOMED formula (Eq. 1) can be split into the energetic (EN) and geometric (GEO) contributions according to the relation proposed by Krygowski and Cyrański (Cyrański et al., 2000)

$$\mathrm{HOMED} = 1 - \left[\alpha\left(R_{\mathrm{ref}} - R_{\mathrm{av}}\right)^2 + \frac{\alpha}{\mathrm{n}}\left(R_{\mathrm{i}} - R_{\mathrm{av}}\right)^2\right] = \\ = 1 - \mathrm{EN} - \mathrm{GEO} \qquad (3)$$

where R_{av} represents the averaged bond length of the investigated benzene ring. An analysis of the evaluated contributions (Fig. 3) showed that the reduction in the HOMED value can be due to either an increase in the bond length alternation (GEO) or an elongation/shortening of the mean bond length of the ring (EN). Mutual comparison of weighted

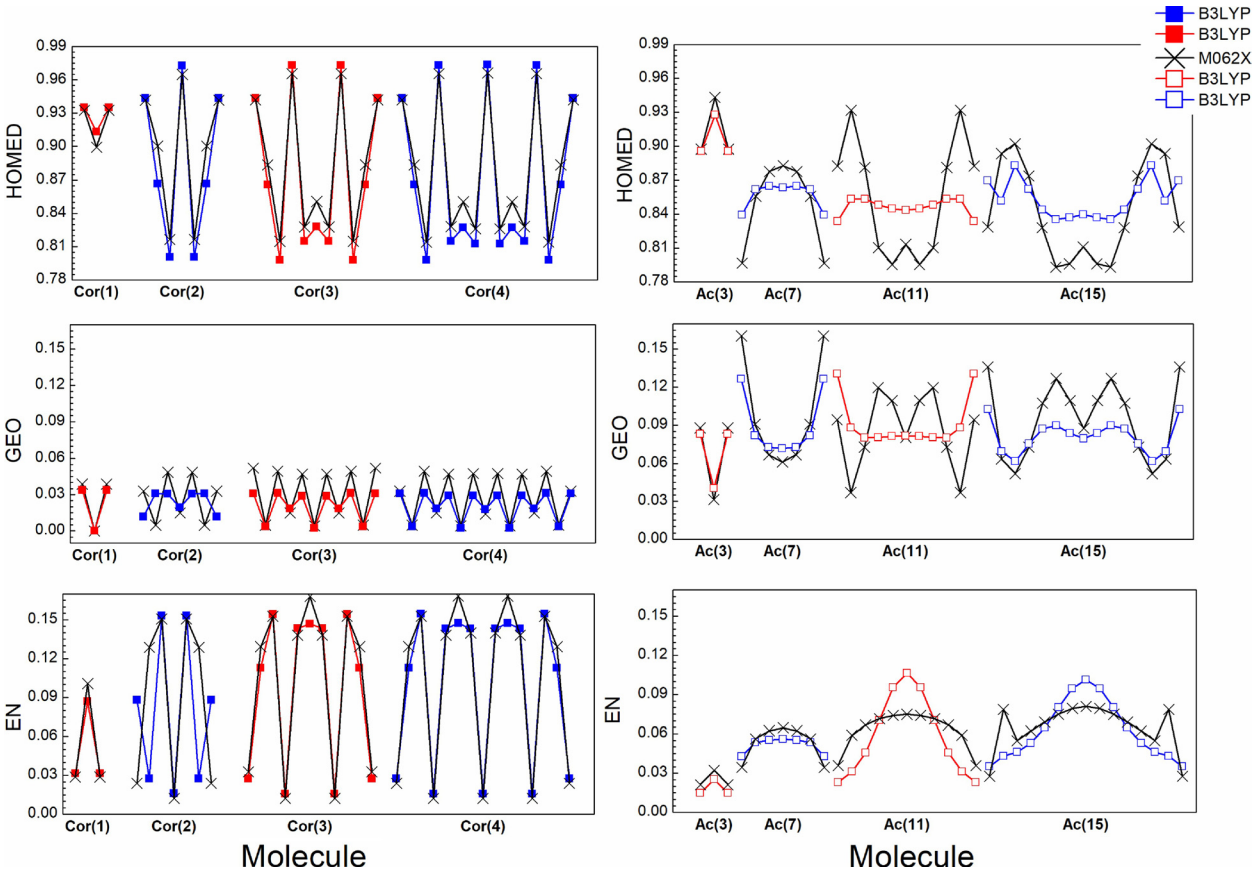

Fig. 3. Schematic representation of trends in studied coronene series (solid symbols) and [n]acenes (open symbols) according to HOMED, GEO and EN indices of central aromatic rings along the longest axial direction (*x*-axis). B3LYP results are indicated by solid and open squares. Cross signs are used for the M06-2X results.

Tab. 1. Separation of B3LYP and M06-2X aromaticity HOMED*/HOMED indices into energetic (EN*/EN) and geometric contributions (GEO*/GEO) for the superrings and rings of studied coronene series.

B3LYP					M06-2X				
Molecule	**Rings**	**HOMED/HOMED***	**EN/EN***	**GEO/GEO***	**Molecule**	**Rings**	**HOMED/HOMED***	**EN/EN***	**GEO/GEO***
Cor(1)	**A**	0.932	0.039	0.029	**Cor(1)**	**A**	0.928	0.039	0.033
Cor(2)	**A/A'**	0.914	0.055	0.031	**Cor(2)**	**A/A'**	0.906	0.058	0.036
	E1	0.965	0.016	0.019		E1	0.973	0.012	0.015
Cor(3)	**A/A'**	0.912	0.058	0.030	**Cor(3)**	**A/A'**	0.906	0.059	0.036
	E1/E1'	0.966	0.016	0.018		E1/E1'	0.973	0.012	0.015
	B	0.893	0.076	0.031		**B**	0.886	0.076	0.038
Cor(4)	**A/A'**	0.912	0.058	0.030	**Cor(4)**	**A/A'**	0.906	0.059	0.036
	E1/E1'	0.966	0.016	0.018		E1/E1'	0.973	0.012	0.015
	B/B'	0.893	0.076	0.031		**B/B'**	0.885	0.076	0.038
	E2	0.966	0.016	0.018		E2	0.974	0.012	0.014

aromaticity parameters for individual superrings in the molecules is presented in Tab. 1. From the quantitative point of view, higher differences in the evaluated indices between the B3LYP and M06-2X functionals were obtained for Ac(11) and Ac(15) molecules.

Accumulative local aromaticity can be described by the sum of HOMED parameters of individual rings of the PAH molecule. Fig. 4 represents the dependence of the sum of HOMED (ΣHOMED), EN (ΣEN) and GEO (ΣGEO) values on the total number of carbon atoms forming the molecule. The accumulative local aromaticity linearly increases with the number of carbon atoms. The slope of the linear dependence of ΣHOMED indices is higher for the coronene series of molecules (see Tab. 2) than in the acenes series for both studied functionals. This observation can be associated with the *peri*-fused six-membered ring inside the coronene unit. Interestingly, slopes of the ΣEN and ΣGEO index dependences for the acene series are almost identical. On the other hand, ΣEN

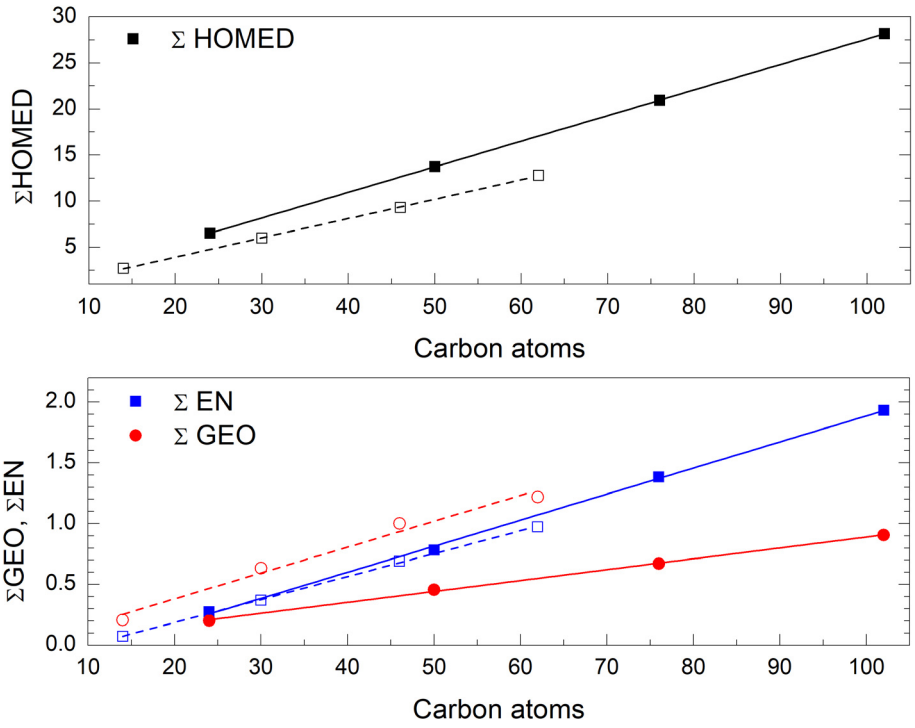

Fig. 4. Dependence of cumulative B3LYP ΣHOMED, ΣGEO and ΣEN indices on the number of carbon atoms for studied coronene series (solid symbols) and [n]acenes (open symbols).

Tab. 2. Parameters for linear dependence of total B3LYP and M06-2X aromaticity indices (ΣHOMED, ΣEN, ΣGEO) on the number of carbon atoms (*x*).

B3LYP	**Function $y = A + B \times x$**			
	Molecule	***A***	***B***	**Correlation coefficient**
ΣHOMED	**Cor**	–0.121 ± 0.019	0.277 ± 0.000	1.0000
	Ac	–0.267 ± 0.095	0.210 ± 0.002	0.9998
ΣEN	**Cor**	–0.258 ± 0.033	0.021 ± 0.000	0.9993
	Ac	–0.190 ± 0.011	0.019 ± 0.000	0.9997
ΣGEO	**Cor**	–0.005 ± 0.014	0.009 ± 0.000	0.9993
	Ac	–0.044 ± 0.089	0.021 ± 0.002	0.9862
M06-2X	**Function $y = A + B \times x$**			
	Molecule	***A***	***B***	**Correlation coefficient**
ΣHOMED	**Cor**	–0.122 ± 0.002	0.276 ± 0.000	1.0000
	Ac	–0.196 ± 0.096	0.207 ± 0.002	0.9998
ΣEN	**Cor**	–0.233 ± 0.003	0.021 ± 0.000	1.0000
	Ac	–0.197 ± 0.009	0.018 ± 0.000	0.9998
ΣGEO	**Cor**	–0.029 ± 0.000	0.011 ± 0.000	1.0000
	Ac	–0.107 ± 0.087	0.024 ± 0.002	0.9898

and ΣGEO index trends for coronene series are concurrent. These dependences show that the aromaticity of single rings is practically independent on the number of other acene/coronene units. In case of the coronene series, the EN term in Eq. 3 is higher than the GEO term, which shows that the aromaticity decreased mainly due to the systematic bond length difference from the reference while the increased bond length alternation has a weaker effect.

Frontier molecular orbitals

Energy levels of frontier molecular orbitals are key parameters in the assessment of the carrier injection ability and stability of materials. Based on the optimised structures of the neutral state, energy levels of the highest occupied (HOMO) and the lowest unoccupied (LUMO) molecular orbitals were calculated. Dependences in these energies on the number of central rings along the longest axial direction are depicted in Fig. 5 for B3LYP, CAM-B3LYP and M06-2X functionals. For the smallest anthracene molecule, **Ac(3)**, the B3LYP HOMO energy is –5.24 eV and it is the highest molecular orbital energy compared with the other studied molecules. The LUMO energy is –1.65 eV. In case of **Cor(1),** the increase of planar p-delocalisation has the minimal effect on the energy value of frontier molecular orbitals, e.g. –5.46 eV for B3LYP HOMO and –1.43 eV for B3LYP LUMO. The HOMO–LUMO energy gap (ΔE_g) value represents another important theoretical parameter corresponding to the electrochemical gap. The B3LYP ΔE_g energy is maximal for the smallest molecules of the studied series (3.59 eV for **Ac(1)** and 4.04 eV for **Cor(1)**) and minimal for the largest ones (0.61 eV and 2.71 eV for **Ac(3)** and **Cor(1)**, respectively). Mutual comparison of the DFT functionals showed that the CAM-B3LYP and M06-2X values of energy gaps, ΔE_g, are approximately two-times higher than those of the B3LYP HOMO–LUMO.

Shapes of the frontier orbitals of the smallest and the largest investigated molecules, anthracene and coronene, reveal the typical π-type molecular orbital character. As it is demonstrated in Fig. 6 for coronene, the lobes of HOMO are spoke-wheel oriented towards the central ring A0. For anthracene, the lobes of HOMO are uniformly delocalised over the longest axial direction. Interestingly, this delocalisation is identical with that of LUMO clouds over A3, A0 and A6 rings for **Cor(1)**. For **Ac(3)**, the lobes of LUMO are mostly delocalised over the bonds parallel with the smaller axial direction. Linear condensation of benzene or superbenzene rings similarly affects the shape of the frontier orbitals. As shown in Fig. 6, the major electron delocalisation is over the nine rings located along the longest axial direction. Moreover, the remaining atoms of the inner superbenzenes in **Cor(4)** also modulate HOMO and LUMO. This indicates different geometrical changes upon the electron abstraction or addition. On the other hand, the shapes and location of nodal planes of depicted frontier orbitals for the largest **Ac(15)** molecule are practically identical. The differences are only in the orbital phases, i.e. in the positive and negative values of the lobes along the shorter axial direction.

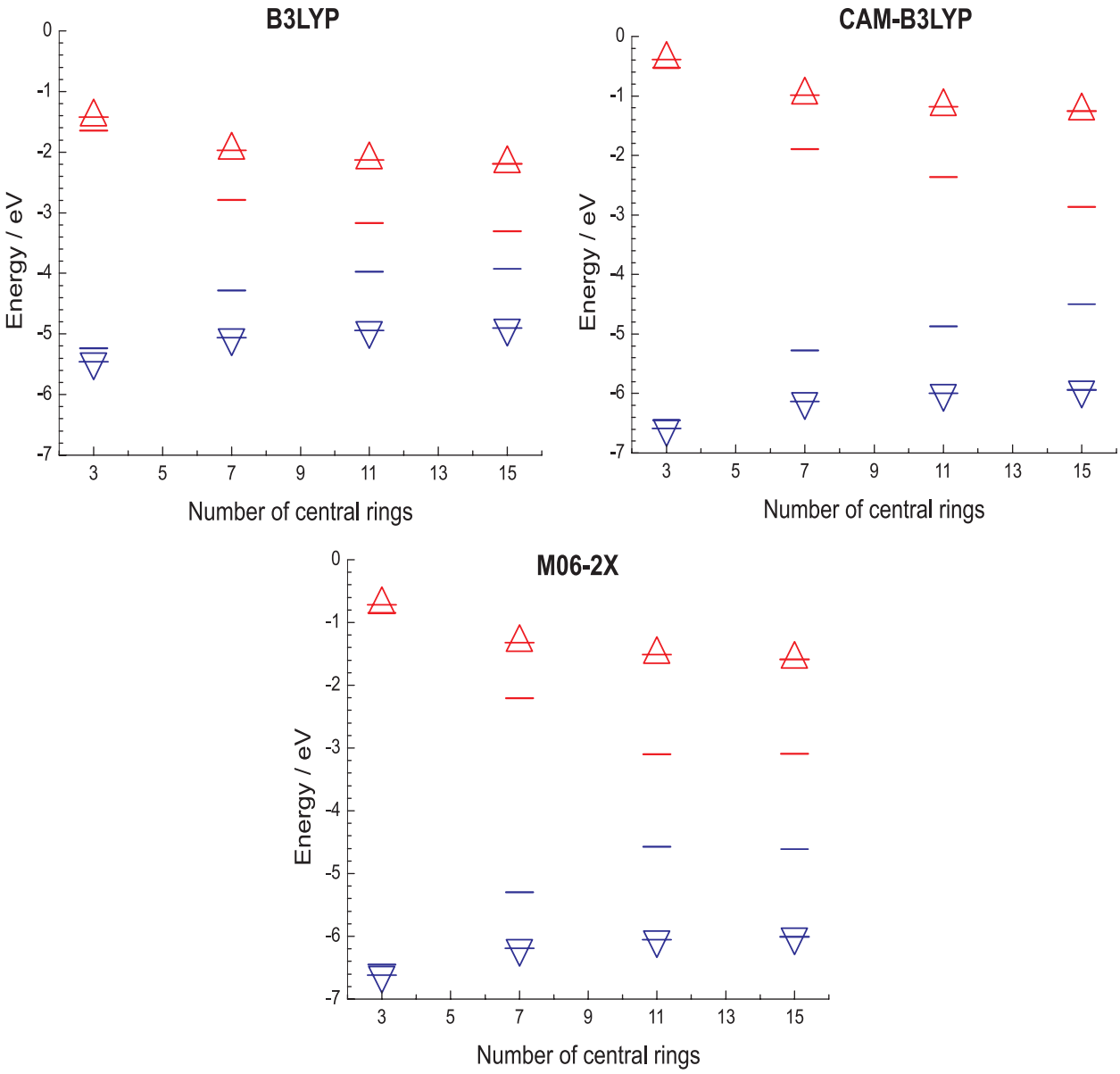

Fig. 5. Energy diagram of B3LYP, CAM-B3LYP and M06-2X frontier molecular orbitals for the studied [n]acenes (bars) and coronene series (up and down triangles). HOMO and LUMO energies are blue and red coloured, respectively.

Finally, it should be noted that the identical shapes of analysed orbitals were obtained for CAM-B3LYP and M06-2X functionals.

Vertical electronic transitions

The longest experimental wavelength electronic singlet transition in the absorption spectrum of acenes ranging in size from anthracene to heptacene, called p band in Clar's (Clar, 1949) or ^1L_a in Platt's (Platt, 1949) nomenclature, and it is due to the HOMO–LUMO transition (Nijegorodov et al., 1997). This band is characterised by vibrational fine structure typical of the acene series. For anthracene, the experimental wavelength is 378 nm (3.28 eV) (Nijegorodov et al., 1997) and for heptacene is 753 nm (1.65 eV) (Einholz et al., 2017). Beside these high-intensity transitions, an additional feature of lower intensity was observed. The value of negligible intensity transition was found at 367 nm (3.38 eV) for anthracene and at 792 nm (1.57 eV) for heptacene. Interestingly, similar features were not observed in the absorption spectra of octacene and nonacene (Tönshoff and Bettinger, 2010). A possible theoretical explanation of the weak features is an electric dipole transition to a state forbidden in the Franck–Condon approximation but increasing intensity, for instance, due to vibronic coupling with the HOMO→LUMO transition. The multi-configuration coupled electron pair approximation (MC-CEPA) (Fink and Staemmler, 1993) level of theory using complete active space self-consistent field reference wave functions with

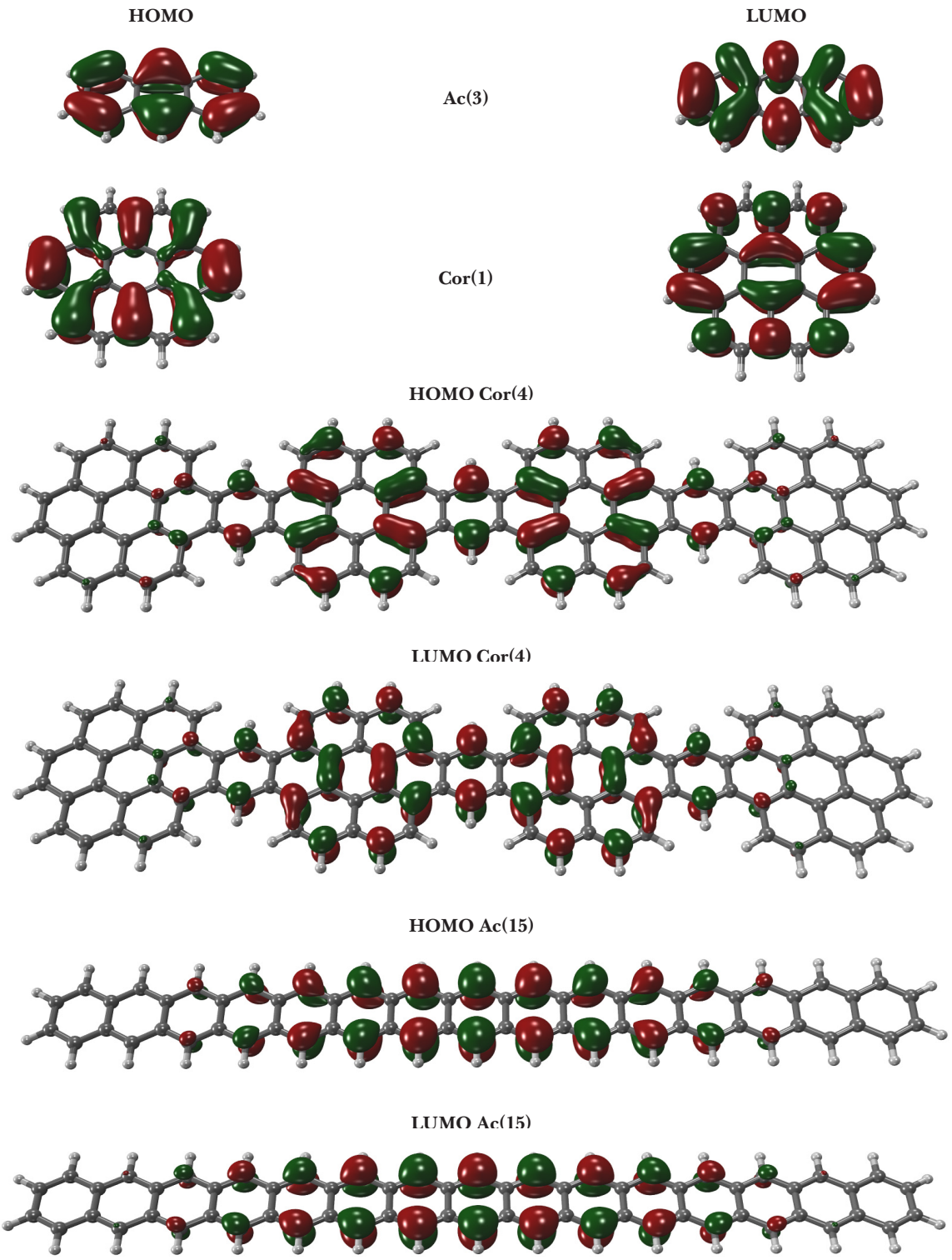

Fig. 6. Shapes of HOMO and LUMO B3LYP molecular orbitals for the smallest and largest studied molecules **Cor(1), Ac(3)** and **Cor(4)**, **Ac(15)**, respectively. Depicted iso-surface value is of 0.025 a.u.

six electrons in six orbitals [CASSCF(6,6)] supported this explanation.

Low-lying ultraviolet visible absorptions of coronene are characterised by three types of valence transitions denoted as α, p-, and β-bands corresponding to electron transitions between two HOMOs and two LUMOs. The experimental absorption spectrum for **Cor(1)** measured in cyclohexane at room temperature exhibits three structured bands modulated by vibronic couplings (Nijegorodov et al., 2001). The determined energies of the individual states are 2.90 eV (428 nm), 3.63 eV (342 nm) and 4.07 eV (305 nm) and the reported experimental oscillator strengths of these electronic states are 0.008,

Tab. 3. TD-DFT energy transitions (in nm/eV) $S_0 \rightarrow S_n$ with the oscillator strength (in parentheses) for studied molecules. Selected functionals are B3LYP, CAM-B3LYP and M06-2X.

				TD-B3LYP					
	Cor(1)[a]	**Cor(2)[a]**	**Cor(3)**	**Cor(4)**		**Ac(3)[b]**	**Ac(7)[b]**	**Ac(12)**	**Ac(15)**
$S_0 \rightarrow S_1$	384/3.229(0.000)	456/2.719(0.052)	498/2.491(0.077)	516/2.404(0.093)	$S_0 \rightarrow S_1$	379/3.274(0.059)	1001/1.239(0.028)	2386/0.520(0.010)	4412/0.281(0.002)
$S_0 \rightarrow S_2$	359/3.453(0.000)	433/2.861(0.008)	451/2.751(0.000)	482/2.573(0.000)	$S_0 \rightarrow S_2$	317/3.905(0.002)	608/2.039(0.000)	1130/1.098(0.000)	2555/0.485(0.001)
$S_0 \rightarrow S_3$	299/4.153(0.663)	393/3.156(0.000)	448/2.768(0.030)	472/2.625(0.000)	$S_0 \rightarrow S_3$	270/4.584(0.000)	546/2.271(0.000)	1014/1.223(0.000)	1170/1.060(0.032)
$S_0 \rightarrow S_4$	299/4.153(0.663)	388/3.199(0.000)	446/2.782(0.000)	453/2.738(0.073)	$S_0 \rightarrow S_4$	249/4.985(0.000)	425/2.918(0.042)	710/1.746(0.000)	1162/1.067(0.000)
$S_0 \rightarrow S_5$	284/4.363(0.000)	383/3.241(0.000)	419/2.958(0.000)	449/2.761(0.028)	$S_0 \rightarrow S_5$	234/5.304(1.905)	421/2.944(0.000)	656/1.889(0.034)	842/1.473(5.406)
				TD-CAM-B3LYP/B3LYP					
	Cor(1)	**Cor(2)**	**Cor(3)**	**Cor(4)**		**Ac(3)**	**Ac(7)**	**Ac(12)**	**Ac(15)**
$S_0 \rightarrow S_1$	355/3.495(0.000)	380/3.259(0.089)	407/3.048(0.154)	416/2.984(0.218)	$S_0 \rightarrow S_1$	342/3.625(0.087)	766/1.619(0.063)	1299/0.955(0.045)	2959/0.419(0.016)
$S_0 \rightarrow S_2$	326/3.801(0.000)	378/3.276(0.005)	386/3.212(0.019)	395/3.138(0.000)	$S_0 \rightarrow S_2$	303/4.087(0.003)	476/2.604(0.000)	780/1.590(0.000)	2315/0.536(0.001)
$S_0 \rightarrow S_3$	266/4.655(0.997)	350/3.542(0.000)	371/3.340(0.000)	389/3.188(0.041)	$S_0 \rightarrow S_3$	235/5.286(0.000)	418/2.967(0.000)	613/2.021(0.000)	820/1.511(0.000)
$S_0 \rightarrow S_4$	266/4.655(0.997)	339/3.653(0.000)	367/3.375(0.000)	377/3.288(0.000)	$S_0 \rightarrow S_4$	226/5.492(0.000)	397/3.126(0.046)	551/2.251(0.032)	799/1.552(0.108)
$S_0 \rightarrow S_5$	259/4.780(0.000)	320/3.874(3.347)	348/3.561(0.018)	367/3.378(0.034)	$S_0 \rightarrow S_5$	224/5.530(2.026)	348/3.562(0.031)	460/2.700(0.002)	706/1.756(7.645)
				TD-M06-2X					
	Cor(1)	**Cor(2)**	**Cor(3)**	**Cor(4)**		**Ac(3)**	**Ac(7)**	**Ac(12)**	**Ac(15)**
$S_0 \rightarrow S_1$	346/3.582(0.000)	371/3.344(0.089)	396/3.130(0.150)	405/3.063(0.209)	$S_0 \rightarrow S_1$	332/3.734(0.083)	743/1.669(0.057)	3060/0.405(0.010)	4614/0.269(0.004)
$S_0 \rightarrow S_2$	315/3.941(0.000)	370/3.347(0.005)	378/3.281(0.015)	386/3.215(0.000)	$S_0 \rightarrow S_2$	297/4.177(0.001)	467/2.654(0.000)	1348/0.920(0.001)	1721/0.720(0.001)
$S_0 \rightarrow S_3$	265/4.687(0.971)	342/3.621(0.000)	364/3.410(0.000)	381/3.257(0.030)	$S_0 \rightarrow S_3$	230/5.381(0.000)	423/2.932(0.000)	638/1.942(0.000)	790/1.569(0.000)
$S_0 \rightarrow S_4$	265/4.687(0.971)	330/3.754(0.000)	360/3.445(0.000)	369/3.356(0.000)	$S_0 \rightarrow S_4$	224/5.532(0.000)	388/3.194(0.024)	577/2.149(6.096)	746/1.661(0.098)
$S_0 \rightarrow S_5$	256/4.845(0.000)	318/3.894(3.227)	340/3.644(0.008)	360/3.442(0.035)	$S_0 \rightarrow S_5$	223/5.554(1.985)	343/3.618(0.027)	540/2.300(0.088)	691/1.794(7.134)

[a]Experimental values of wavelength are of 428 nm (2.90 eV), 342 nm (3.63 eV) and 305 nm (4.07 eV) for **Cor(1)** and of 248 nm (5.00 eV), 333 nm (3.72 eV) and 445 nm (3.65 eV) for **Cor(2)**.

[b]Experimental values of wavelength are of 378 nm (3.28 eV) and 367 nm (3.38 eV) for anthracene **Ac(3)** and of 753 nm (1.65 eV) and 792 nm (1.57 eV) for heptacene denoted as **Ac(7)**. The second one has lower intensity.

0.670 and 4.900, respectively. The enormous value of 4.900 can be explained by the superaromaticity imparted by the ring of sextets of coronene. Also, oscillator strengths are dependent on temperature due to the symmetry perturbation of the coronene molecule. In case of **Cor(2)**, three experimental structured band systems were identified at 248 nm (5.00 eV), 333 nm (3.72 eV) and 445 nm (2.79 eV) when the sample was trapped in solid inert-gas matrices (Ruiterkamp et al., 2002). The corresponding relative intensities are 87:100:76. Spectral peaks are slightly red shifted to those observed for dicoronylene in 1,2,4-trichlorobenze solution (Lempka et al., 1985), i.e. 506 nm (2.45 eV), 369 nm (3.36 eV) and 340 nm (3.65 eV).

The calculated electronic gas-phase transition energies and oscillator strengths for the first five lowest vertical excited states of studied molecules are collected in Tab. 3. For the simplest **Cor(1)**, the first two optical transitions have negligible oscillator strengths compared with the energetically equivalent third and fourth electronic transitions at 299 nm (TD-B3LYP), 266 nm (TD-CAM-B3LYP) and 265 nm (TD-M06-2X). Contrary to the acene molecules, the TD-DFT approach provides correct order of the electronic excited states for the **Cor(1)** and **Cor(2)** molecules. However, precise interpretation of the experimental spectrum should include vibronic couplings between the electronic states. Therefore, direct comparison of the theoretical line spectra with experimental data is problematic.

Interestingly, the HOMO→LUMO transition does not occur in the first electronic excitation of all three functionals. A consecutive addition of superbenzene rings increases the oscillator strength of the lowest excitation energy where the HOMO→LUMO transition dominates. For example, the TD-B3LYP $S_0 \rightarrow S_1$ transitions are 456 nm for **Cor(2)**, 498 nm for **Cor(3)** and 516 nm for **Cor(4)**. In case of the reference acene series, the lowest $S_0 \rightarrow S_1$ transition of **Ac(3)** and **Ac(7)** have higher oscillator strength than the other three/two transitions. Also, this transition originates in the frontier HOMO and LUMO. Linear elongation of the molecular structure significantly decreases the oscillator strength of the lowest energy transition. As shown in Tab. 3, in case of the **Ac(3)** molecule, the TD-B3LYP energy of the lowest transition of 379 nm (3.27 eV) is in very good agreement with the experimental value of 378 nm (3.28 eV). Although the TD-B3LYP optical transitions are in better agreement with the experimental observations for the **Cor(1)** and **Cor(2)** molecules, the CAM-B3LYP and M06-2X functionals estimate the lowest excitation energies more accurately for acenes.

The interesting correlation of HOMO–LUMO energy gaps, ΔE_g, with the $S_0 \rightarrow S_1$ energies of the B3LYP functional is demonstrated in Fig. 7.

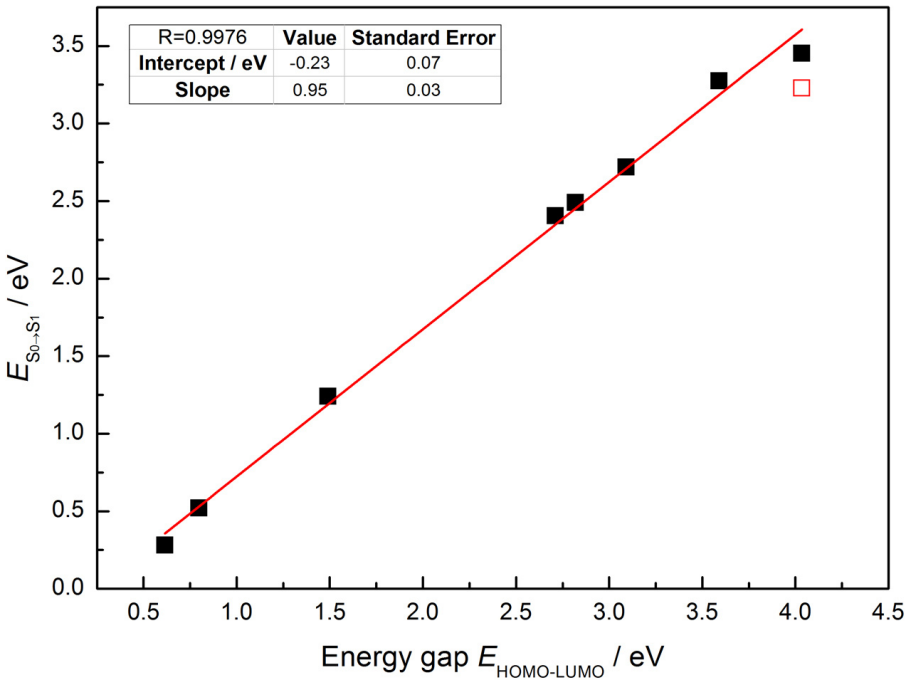

Fig. 7. Dependence of TD-B3LYP HOMO→LUMO (black solid squares) transition energy on energy HOMO-LUMO gaps for the studied [n]acenes and coronenes series. Outlier (red hollow square) represents the $S_0 \rightarrow S_1$ transition for **Cor(1)** molecule, which does not correspond to the HOMO→LUMO transition. Table includes parameters of linear regression. R is the correlation coefficient.

The TD-B3LYP $S_0 \rightarrow S_1$ correspond to the HOMO→LUMO transition for all studied molecules excluding **Cor(1)**. In case of **Cor(1)**, the $S_0 \rightarrow S_2$ energy was applied instead of the $S_0 \rightarrow S_1$ one, where the HOMO→LUMO transition dominates. The obtained dependence is linear with a sufficiently high correlation coefficient. Similar linear dependences were also obtained for the other DFT functionals. Regression parameters including the intercept, slope, standard errors and correlation coefficient are 1.1 ± 0.1 eV (–0.9 ± 0.2 eV), 1.17 ± 0.05 (0.78 ± 0.04) and 0.9946 (0.9923) for the TD-M06-2X (TD-CAM-B3LYP) calculations.

Conclusions

Using the density functional theory, structural and electronic properties of coronene and three linear *cata*-benzocoronene oligomers were studied. Local aromaticity of six-membered rings along the longest axial direction as well as of superbenzene and its connecting rings was discussed employing HOMED, EN and GEO aromaticity descriptors. In case of the benzocoronene oligomers, local aromaticity of individual superbenzene central aromatic rings has oscillating character. On the other hand, the highest B3LYP HOMED parameters, which are practically independent on molecular length, were found for the smallest connecting benzene rings between the superbenzene units. For the largest model of [n]acenes (n = 15), the inner rings are less aromatic than outer ones. Linear dependence of the sum of HOMED, EN and GEO indices on the number of carbon atoms was found for B3LYP and M06-2X geometries. Slopes for the HOMED parameters dependences on the number of carbon atoms for **Cor(n)** are by about 25 % higher than for the acenes. On the other hand, for ΣGEO dependences the slopes are by 25 % lower for the coronene series than for the acenes series of molecules. Interestingly, only the slopes of ΣEN indices for both molecules are almost identical. Most interesting are the almost identical slopes of ΣEN and ΣGEO dependences in the acenes series. The obtained theoretical data show that local aromaticity of the individual rings in the superbenzene is strongly dependent on the position within the oligomeric chain. Moreover, the shapes of the frontier molecular orbitals indicate the geometrical changes upon the abstraction or addition of electron for **Cor(4)** compared with **Ac(15)**. This behaviour is interesting in the application of **Cor(n)** molecules in opto-electronic devices.

Acknowledgment
This work has been supported by the Slovak Grant Agency (1/0601/15) and the Slovak Research and Development Agency (APVV-15-0053). We are grateful to the HPC centre at the Slovak University of Technology in Bratislava, which is a part of the Slovak Infrastructure of High Performance Computing (SIVVP project, ITMS code 26230120002, funded by the European Region Development Funds, ERDF) for the computational time and resources provided.

References

Aihara J (2003) Chem. Phys. Lett. 381 (1—2): 147—153, doi: 10.1016/j.cplett.
Anusooya Y, Chakrabarti A, Pati SK, Ramasesha S (1998) Int. J. Quantum Chem. 70: 503.
Bayrakçeken F, Keskin AU (2004) Asian J Spectrosc. 8(1): 9—14.
Becke AD (1988) Phys Rev A 38: 3098—3100.
Behrens S, Köster AM, Jug K (1994) J. Org. Chem. 59: 2546.
Brock CP, Dunitz JD (1990) Acta Crystallographica Section B46: 795—806.
Clar E (1939) Chem. Ber. 72: 1817.
Clar E. (1949) Chem. Ber. 82: 495.
Cyrański MK, Krygowski TM, Katritzky AR, Schleyer PVR (2002) J. Org. Chem. 67: 1333—1338. doi: 10.1021/jo016255s.
Cyranski MK, Stepień BT, Krygowski TM (2000) Tetrahedron 56: 9663.
Dabestani R, Ivanov IN (1999) Photochem. Photobiol. 70: 10.
Fetzer JC (2000) The Chemistry and Analysis of the Large Polycyclic Aromatic Hydrocarbons. New York: Wiley.
Fink R, Staemmler V (1993) Theor. Chim. Acta 87: 129.
Flukiger P, Luthi HP, Sortmann S, Weber J (2002) Molekel 4.3, Swiss National Supercomputing Centre, Manno, Switzerland.
Frisch MJ, Trucks GW, Schlegel HB, Scuseria GE, Robb MA, Cheeseman JR, Scalmani G, Barone V, Mennucci B, Petersson GA, Nakatsuji H, Caricato M, Li X, Hratchian HP, Izmaylov AF, Bloino J, Zheng G, Sonnenberg JL, Hada M, Ehara M, Toyota K, Fukuda R, Hasegawa J, Ishida M, Nakajima T, Honda Y, Kitao O, Nakai H, Vreven T, Montgomery JA Jr., Peralta JE, Ogliaro F, Bearpark M, Heyd JJ, Brothers E, Kudin KN, Staroverov VN, Keith T, Kobayashi R, Normand J, Raghavachari K, Rendell A, Burant JC, Iyengar SS, Tomasi J, Cossi M, Rega N, Millam JM, Klene M, Knox JE, Cross JB, Bakken V, Adamo C, Jaramillo J, Gomperts R, Stratmann RE, Yazyev O, Austin AJ, Cammi R, Pomelli C, Ochterski JW, Martin RL, Morokuma K, Zakrzewski VG, Voth GA, Salvador P, Dannenberg JJ, Dapprich S, Daniels AD, Farkas O, Foresman JB, Ortiz JV, Cioslowski J and Fox DJ (2009) Gaussian 09, Revision D.01, Gaussian, Inc. Wallingford CT.
Frizzo CP, Martins MA (2012) Struct. Chem. 23(2): 375—380.
Furche F, Ahlrichs R (2002) J. Chem. Phys. 117: 7433—7447. doi: 10.1063/1.1508368.
Hariharan PC, Pople JA (1973) Theor. Chim. Acta. 28:213—222. doi: 10.1007/BF00533485.
Haynes WM (2011) In: CRC Handbook of Chemistry and Physics (92nd ed.). Boca Raton, FL: CRC Press. p. 3.128. ISBN 978-1-4398-5511-9.

Hohenberg W, Kohn P, Hohenberg P, Kohn W (1964) Phys. Rev. 136: B864—B871. doi: 10.1103/PhysRev.136.B864.
Howard ST, Krygowski TM (1997) Can. J. Chem. 75: 1174.
Jinno K, Miya S, Sasaki S-I, Fetzer JC, Biggs WR (1990) Fourth Symposium on our Environment Proceedings of the Fourth Symposium on Our Environment, held in Singapore.
Krygowski TM, Cyrański MK (2001) Chem. Rev. 101: 1385.
Lee C, Yang W, Parr RG (1988) Phys. Rev. B 37: 785— 789.
Lempka HJ, Obenland S, Schmidt W (1985) Chem. Phys. 96(2): 349—360.
Ligabue A, Pincelli U, Lazzeretti P, Zanasi P (1999) J. Am. Chem. Soc. 121: 5513.
Mackay D, Callcott D (1998) A. Neilson (ed.). PAHs and Related Compounds. The Handbook of Environmental Chemistry. (pp. 325—345). Springer, Berlin Heidelberg. ISBN 978-3-642-08286-3.
Moyano A, Paniagua JC (1993) Trends Org. Chem. 4: 697.
Nijegorodov N, Mabbs R, Downey WS (2001) Spectrochimica Acta Part A 57: 2673—2685.
Nijegorodov N, Ramachandran V, Winkoun DP (1997) Spectrochim. Acta A 53: 1813.
Ośmiałowski B, Raczyńska ED, Krygowski TM (2006) J. Org. Chem. 71: 3727—3736. doi: 10.1021/jo052615q.
Platt JRJ (1949) Chem. Phys. 17: 484.
Portella G, Poater J, Bofill JM, Alemany P, Sola M (2005) J. Org. Chem. 70: 2509—2521.
Potticary J, Jensen TT, Hall SR (2017) Sci. Rep. 7(1): 9867.
Potticary J, Terry LR, Bell C, Papanikolopoulos AN, Christianen PCM, Engelkamp H, Collins AM, Fontanesi C, Kociok-Kohn G, Crampin S, Da Como E, Hall SR (2016) Nat. Comm. 7: 11555.
Randic M (2003) Chem. Rev. 103: 3449.
Rassolov VA, Pople JA, Ratner MA, Windus TL (1998) J. Chem. Phys. 109: 1223—1229. doi: 10.1063/1.476673.
Ruiterkamp R, Halasinki T, Salama F, Foing BH, Allamandola LJ, chmidt W, Ehrenfreund P (2002) A&A 390: 1153—1170.
Runge E (1984) Phys. Rev. Lett. 52: 997—1000. doi: 10.1103/PhysRevLett.52.997
Schleyer PvR, Manoharan M, Jiao HJ, Stahl F (2001) Org. Lett. 3: 3643.
Steiner E, Fowler PW (1996) Int. J. Quantum Chem. 60: 609.
Tönshoff C, Bettinger HF (2010) Angew. Chem. 49: 4125.
Yanai T, Tew D, Handy N (2004) Chem. Phys. Lett. 393: 51—57. doi: 10.1016/j.cplett.2004.06.011.
Zhao Y, Truhlar DG (2008) Theor. Chem. Acc. 120: 215—241. doi: 10.1007/s00214-007-0401-8.